

Survey for Emission-Line Galaxies: Universidad Complutense de Madrid List 3 ¹

O. Alonso², C. E. García-Dabó, J. Zamorano, J. Gallego, M. Rego
Dpto. Astrofísica, Universidad Complutense de Madrid, E-28040 Madrid, Spain

ABSTRACT

A new low-dispersion objective-prism search for low-redshift ($z < 0.045$) emission-line galaxies (ELG) has been carried out by the Universidad Complutense de Madrid with the Schmidt Telescope at the Calar-Alto Observatory. This is a continuation of the UCM Survey, which was performed by visual selection of candidates in photographic plates via the presence of the $H\alpha + [NII]\lambda 6584$ blend in emission. In this new list we have applied an automatic procedure, fully developed by us, for selecting and analyzing the ELG candidates on the digitized images obtained with the MAMA machine. The analyzed region of the sky covers 189 square degrees in nine fields near $\alpha = 14^h$ & 17^h , $\delta = 25^\circ$. The final sample contains 113 candidates. Special effort has been made to obtain a large amount of information directly from our uncalibrated plates by using several external calibrations. The parameters obtained for the ELG candidates allow for the study of the statistical properties for the sample.

Subject headings: galaxies: general, surveys, starburst — techniques: image processing — Surveys —

¹Based on observations collected at the German-Spanish Astronomical Center, Calar Alto, Spain, operated jointly by the Max-Planck Institut für Astronomie (MPIA), Heidelberg, and the Spanish National Commission for Astronomy.

²present address: Dpto. Arquitectura de Computadores y Automática, Universidad Complutense de Madrid, E-28040 Madrid, Spain

1. Introduction

The Universidad Complutense de Madrid Survey (UCM Survey) has been carried out during the last several years with the aim of looking for H α emission-line galaxies. It is described in detail by Zamorano et al. (1994, 1996), in UCM Lists 1 & 2.

The UCM Survey was initiated with several objectives, the main goals being: (1) to identify and study new young, low-metallicity galaxies; (2) to carry out the classification and determination of the overall properties and completeness of the sample of emission-line galaxies (ELGs) selected; (3) to determine the spatial distribution and luminosity function of the new galaxy population. We also wished to compare our survey with others and to find out differences between the sample obtained with various objective-prism techniques and to study the overall relation between the far-infrared properties and the optical behavior of the star-forming galaxies. Finally, we intended to determine the evolutionary status and the different underlying stellar populations of the objects in order to detect any effect of evolution in the starburst phenomena and to quantify the properties of the star formation in the local universe.

The final product of Lists 1 and 2 was the Universidad Complutense de Madrid (UCM) sample of star-forming galaxies in the local Universe. This sample has been observed and analyzed in detail (optical imaging: Vitores et al. (1996a, 1996b); spectroscopy: Gallego et al. (1996, 1997); near infrared imaging: Alonso-Herrero et al. (1996), Gil de Paz et al. (1998)) and has provided the luminosity function for the star-forming galaxies and the density of star formation rate in the local Universe (Gallego et al. 1995).

Lists 1 and 2 suffer from the subjective technique of looking for candidates by visual inspection of the plates through a 10 \times binocular microscope. We intend to overcome this drawback by automatic selection on the digitized plates. This method was shown to provide good performance and improvement in the selection of candidates by applying it to several fields (Alonso et al. 1995; Alonso 1996). In this work we present the UCM List 3 obtained after using the automatic detection process in nine contiguous fields covering 189 sq. deg.

Section 2 describes the instrumental setup and observations. In section 3 the method used to select the candidates is outlined. Section 4 presents several parameters measured for every galaxy of the sample and

explains the way they were obtained. In section 5 the known selection effects are discussed. Finally, some statistical properties and a comparison with other surveys are presented in section 6 and 7, respectively.

2. Observational Data

This survey is based on photographic plates obtained with the 80/120 cm f/3 Schmidt Telescope of the Calar Alto German-Spanish Observatory (Almería, Spain) (Birkle 1984) in June 1993. All the fields acquired for this research were obtained using the direct and objective-prism configurations. In both modes, we use 8 \times 10 inch² plates, covering an useful field of 4.4 \times 5.5 deg² with a plate scale of 86'' mm⁻¹. They were hypersensitized by baking them in an atmosphere of forming gas for 2 hr prior to exposure. Full details of the plates are listed in table 1.

Direct plates were obtained exposing IIIaJ plates, combined with the GG385 filter, for 1 hour. This configuration gives an instrumental response similar to the Johnson B band. Prism plates were acquired in the red region of the spectrum. The use of IIIaF emulsion, with a sharp red cutoff at 6850Å, and a RG630 filter provides an useful spectral range from \sim 6400 to 6850Å. The objective-prism plates were obtained through a full aperture 4° prism that yields a dispersion of 1980Å mm⁻¹ at H α (see §4.3). Dispersion of the prism spectra runs N-S axis. Our experience with the instrumental setup used indicates that exposures two hours long are a good balance between depth and plate background. This instrumental configuration registers the H α + [NII]³ blend in emission for objects up to $z \approx 0.045$.

Quality standards for the analyzed plates are good seeing, no cloud interference, no exposure interruption and telescope near the meridian. Excellent guiding was achieved on this observing run by the use of the new automatic guiding system installed on the Schmidt Telescope.

The plates were scanned using the MAMA⁴ machine, a high performance multichannel microdensitometer located at the Observatoire de Paris (Guibert & Moreau 1991; Moreau 1992). We used a pixel size and sampling step of 10 μ m, the highest resolution achieved by the machine. Each scanned plate returns a 23k \times 18k pixel image at 0.86'' pix⁻¹.

³ The combined H α + [NII] emission will be referred to in what follows as simply the H α emission.

⁴ MAMA (Machine Automatique à Mesurer pour l'Astronomie)

Figure 1 shows the fields covered by this discovery list. They are placed in two regions located in the areas $13^h45^m < \alpha < 14^h55^m$; $21^\circ < \delta < 27^\circ$ and $16^h25^m < \alpha < 17^h50^m$; $21^\circ < \delta < 27^\circ$. The total surveyed area is 189 deg^2 .

3. Data reduction and selection of candidates

In order to decrease the uncertainties intrinsic to visual scanning, we have developed a new method for the automatic selection of emission-line candidates in digitized objective-prism plates. The full procedure is described in detail in Alonso et al. (1995) and Alonso (1996). Here we point out a brief discussion of the method.

The first task must be to find all the objects on the plates. To locate and measure objects in the astronomical images we have developed a program that performs this job by thresholding the image a certain number of sigma over the local sky background. It returns a catalogue with several parameters as positions, sizes, fluxes, etc. for all the identified objects with a minimum selectable size. Our BUHOFITS software is able to handle large FITS files up to our $23k \times 18k$ pixel images. The large amount of spurious identifications due to emulsion flaws, plate scratches or satellite tracks are rejected by cross-correlating the catalogues obtained from direct and prism plates for the same field. We have used a plot of the logarithm of the area versus density flux to discern between stellar-like and extended objects (Reid & Gilmore 1982).

Subsequently the spectrum of all the objects are extracted by adding the central five scans (i.e., those with higher signal), from the objective-prism image. These monodimensional spectra are obtained in arbitrary and instrumental density units. No calibration spots were recorded on the plates to obtain a photographic density to intensity relation. Nevertheless the emission feature is clearly registered in these uncalibrated spectra and will be used in all the subsequent analysis. Due to the spectrum extraction procedure it can be noted that we are missing those galaxies with emission out of the central region. This is one of our selection effects, but it only affects very bright, extended and well known galaxies.

The emission-line galaxy candidates are selected by analyzing the prism spectra for all the objects. We use

three different criteria in order to perform this selection, as is described in detail in Alonso et al. (1995). In our low dispersion and uncalibrated plates, all the spectra show a similar appearance, mainly dominated by the instrumental response. Only objects showing the $H\alpha$ line in emission will present a clear discrepancy with respect to the continuum spectra of stars and galaxies without emission. The selection criteria are based in this fact, and allow to compute a selection index for each object that informs us about the reliability of the presence of an emission feature. The final sample is obtained after visual inspection of those objects with largest selection index. This step is needed because several different configurations like overlapping stars, emulsion scratches in the prism image, etc., can produce extracted spectra with an apparent strong emission feature.

The UCM survey had a typical success of 70% when looking for ELGs (Lists 1 and 2). The remaining 30% were confirmed to be objects showing no emission. The automatic method has proved to improve these results (Alonso et al. 1995; Alonso 1996). In these studies we have compared the samples of ELG obtained after visual and automatic search in two fields. The new technique recovers nearly 80% of the objects detected by visual scanning. All of the objects not recovered by the automatic method are extended and very bright galaxies or galaxies with emission knots out of the nucleus. Moreover, with the automatic method we see an enhancement in the number of confirmed candidates selected. As it is shown in Alonso et al. (1995) and Alonso (1996) an increase of 24% in the total number of objects with confirmed $H\alpha$ emission has been reached with respect to the visual inspection.

4. Physical Parameters

We have put special attention into improving the extraction of information from our uncalibrated photographic plates. Several parameters have been obtained with intermediate accuracy for all the candidates. Table 2 presents the full information for the objects of the third list of our survey. Column (1) contains the name of the galaxy according to the IAU rules. Equatorial coordinates for J2000.0 are given in columns (2) and (3). Column (4) presents an estimate of the B magnitude obtained from our photographic plates (see §4.4). In columns (5) and (6) we present the size at the $25 \text{ mag arcsec}^{-2}$ isophote, in arcsec,

is developed and operated by CNRS/INSU (Institut National des Sciences de l'Univers) and located at the Observatoire de Paris

and the position angle (see §4.2). Estimated redshifts are listed in column (7) (see §4.3). Column (8) gives a preliminary morphological classification derived by visual analysis of the Digitized Sky Survey⁵ (DSS) images, whereas column (9) classifies each candidate into three categories according to the strength of the emission seen in the prism plates. The meaning of the codes used in these columns are presented in the caption of the table. Finally, column (10) shows previous designations of the candidates. Finding charts from the DSS are included in figure 12.

The parameters listed in the table are estimations, since spectroscopic and photometric studies have not been carried out. Because our uncalibrated plates do not permit us to directly obtain absolute parameters for the objects, we have performed several external calibrations by relating our photographic parameters with calibrated data for a small subsample of objects obtained from different catalogues. However this approximation does not allow high accuracy and some of the calibrations are not even possible. This occurs if we try to measure the $EW(H\alpha)$ in our spectra, for which we will need a density to intensity calibration and, more important, a large sample of emission-line galaxies with known $EW(H\alpha)$ for each plate in order to obtain a well sampled relation.

Next we briefly describe the procedure followed for obtaining each parameter.

4.1. Astrometry

We follow a standard procedure performed during the plate scan by the MAMA machine in order to derive the constants for the plate astrometry. A third-order polynomial transformation is derived by using astrometric reference stars from the PPM catalogue (Roeser & Bastian 1991). The rms in the residuals of the astrometric reductions are about $0.3''$, although large deviations can be achieved for very extended objects with several components. Columns (2) and (3) of table 2 catalogue the coordinates of the candidates referred to the equinox J2000.0.

⁵The Digitized Sky Survey were produced at the Space Telescope Science Institute under U.S. Government grant NAG W-2166. The images of these surveys are based on photographic data obtained using the Oschin Schmidt Telescope on Palomar Mountain and the UK Schmidt Telescope. The plates were processed into the present compressed digital form with the permission of these institutions.

4.2. Sizes and Position Angles

During the object scanning process, we obtain the photographic major and minor axis and the position angle for each detected object by fitting an ellipse to pixels with a photographic density 3σ over the local plate background. The sizes of a galaxy measured directly in the plate cannot be straightforwardly converted to sizes in arc-seconds via the plate scale because of the photographic plate behavior. An ideal point of light is spread on the photographic emulsion over a wide area, and this effect grows with the source brightness. Hence, the size measured directly on the plate is a function of the real size of the source, the magnitude, also the luminosity profile for an extended source. We have calibrated our photographic sizes with known galaxies, using the Catalogue of Principal Galaxies (PGC) in its electronic version Extragalactic Card Index System (ECIS) (Paturel et al. 1989). This catalogue has the advantage of being homogeneous, where sizes are all referred to the isophote 25 mag arcsec⁻² (Paturel et al. 1987). In figure 2 we show the calibration derived for a single field. The other plates follow similar relations.

Figure also shows that the instrumental MAMA sizes are systematically smaller than such obtained from the PGC. This fact is due to both the notably less depth of our photographic plates and the method used to obtain the sizes (thresholding the image 3σ over the local background). Nevertheless, the calibrations derived allow us to estimate the size of our candidates within an uncertainty of $20''$. Higher precision could be achieved with more homogeneous data. In Alonso (1996) an error of $2''$ was obtained calibrating with photometry for the UCM galaxies (Vitores et al. 1996b).

The position angle is adopted as the orientation of the fitted ellipse. There is no need for a calibration with external data, but a checking was made using the same ECIS catalogue cited above. This provided an estimation of the error, being 8° for 1σ . For very elongated galaxies the error should be notably smaller.

4.3. Redshift

The measurement of the redshift of the ELG candidates in our photographic plates requires a wavelength calibration of the spectra. This calibration involves obtaining the prism dispersion and requires the knowledge of a reference point at a specific wavelength for each spectrum.

The prism disperses the light by means of the changing refractive index with the following dependence on wavelength, in first order:

$$n(\lambda) = a + \frac{b}{\lambda^2} \quad (1)$$

where a, b are two constants. Thus, the position of a certain spectral feature in the objective-prism image will follow the same dependency:

$$x(\lambda) = A + \frac{B}{\lambda^2} \quad (2)$$

Here, the A constant depends on the reference point we choose, whereas the B constant is only related to the characteristics of the prism.

In order to obtain the dispersion curve for the 4° objective prism of the Calar-Alto Schmidt Telescope a test plate was taken. The configuration used was IIIaF emulsion without a filter. With a short exposure the prism spectra of several bright stars were registered, covering a spectral range from the blue atmospheric cut-off until 6850\AA due to the sharp red cut-off of the IIIa-F emulsion. The dispersion curve was obtained by measuring the position of the strong absorption Balmer lines of A stars. Fitting the data to the following expression (Alonso 1996) (see figure 3)

$$\frac{d\lambda}{dx} = -\frac{\lambda^3}{2B} \quad (3)$$

yields a value of $B = (-713 \pm 2) \cdot 10^8 \text{\AA}^2 \mu\text{m}$. To measure the wavelength of the $H\alpha$ feature in the prism spectra we also need the knowledge of a reference point. The emulsion red cut-off at $\sim 6850\text{\AA}$ can not be used due to its high dependency with brightness, color and size. We have used instead the astrometric reduction to obtain a constant reference point for all the spectra. This point is obtained by converting the position of the object from the direct to the prism plate. We do not know the wavelength of this reference point, but it will be the same for all the spectra, even for different plates, where we have applied the same astrometric reduction, and it will not be affected by the effects previously noted (size, brightness and color). Only when the emission comes out of center of the galaxy the method clearly fails. Two identical galaxies showing $H\alpha$ emission, the first one in the nucleus and the second one in an external knot would show the emission line in different location of their prism spectra

with respect to a same reference point, obtained from the plate to plate transformation. Therefore this fact would yield an erroneous value of the redshift for the second one.

In order to obtain the wavelength of this reference point, that is, the value of the constant A we represent the redshift (z) of known galaxies with respect to the $H\alpha$ position in the prism spectrum, relative to the reference point (Δx). This relation must follow the expression:

$$z = \frac{\sqrt{\frac{B}{\Delta x(\mu\text{m}) - A}} - \lambda_0}{\lambda_0} \quad (4)$$

where λ_0 is 6562.8\AA if we are working with the $H\alpha$ line. Therefore we can calculate the value of A by applying an algorithm of minimum squares to the data. The value of such constant, obtained separately for the nine fields, yields the same results inside 1σ error bar, confirming the procedure.

Assuming an uncertainty of 1 pixel in the determination of the center of the line, and taking into account the rms in the calibration fit, the typical error in the computation of the redshift results 0.004 for 1σ (i.e. 1200 km s^{-1}). In figure 4 we present the data obtained applying the method just described for an small subsample of galaxies with known redshifts in order to test our procedure. The galaxies showing large deviations are explained noting that the method may fail when the galaxy is very extended and the emission feature comes from a external knot. This is the case of UCM1436+2245 (IRAS 14360+2245), with a redshift of 0.04 (Fisher et al. 1995). If we apply our method it gives an estimate of $z=0.017$ due to the presence of a double component emission probably originating in different knots. Column 7 of Table 2 presents the redshift obtained for non-catalogued candidates. Data marked with an asterisk are obtained from literature.

Obviously, these redshifts are based in the assumption that the emission feature registered in the prism spectra is the $H\alpha$ line. This conjecture is based in the fact that none of the confirmed emission-line galaxies from the previous UCM lists 1 & 2 was revealed as distant galaxies with their emission lines redshifted to our spectral coverage. In addition, a galaxy with a $M^* = -21.4$ magnitude, located at $z=0.3$ will show the [OIII]5007 line in the $H\alpha$ region, but the apparent magnitude would be notably fainter than the limit of our prism plates ($m_r \approx 18$).

4.4. Magnitudes

The direct plates were obtained with an instrumental response near the B band of the Johnson system, and therefore we are interested in measuring the magnitudes of our ELG sample. Our plates are not calibrated, but we can relate the photographic flux, the sum of the density for all the pixels of the image, with the B magnitude for objects recovered from databases. This relation works fine for stellar objects ($\sigma \approx 0.1$ mag), but it is not straightforward to apply to extended objects because the dependence with the size of the source. Using both photographic density and size it is possible to estimate the magnitudes, but with larger errors, up to 0.5 mag for very extended galaxies.

Several studies have been published which have achieved better accuracy using photographic plates, but in general all of them require calibration spots (Surace & Comte 1994) or the calibration give good results only in photometry for stellar-like objects (Kroll & Neugebauer 1993; Berger et al. 1991; Mohan & Crezé 1987). In general, the photometry of extended sources has several sources of error sometimes hard to correct for (see de Vaucouleurs 1984)).

B magnitudes listed in column (4) of table 2 are derived using the method just described above, and should be used only as estimates for statistical or observational purposes. Only values for compact galaxies can be taken with greater confidence.

5. Selection effects

One of the major problems encountered when working with photographic plates is that the characteristics of each of them can vary notably with respect to the other ones, even taking special care in repeating all the observational setup, being almost impossible to obtain a homogeneous sample of galaxies. In order to understand the biases of our observational procedure, we have compared the samples of galaxies obtained in our survey with those recovered by using different observational configurations. This job is presented in detail in Zamorano et al. (1994, 1996) for the UCM Lists 1 & 2, and is also presented in section 7 of this paper for this new List 3.

Nevertheless in this section we have used the spectroscopic data derived for the two previous lists of the UCM survey (Gallego et al. 1995) with the aim of investigating the observational biases of our instrumental configuration. This analysis (Alonso 1996) shows

that neither the equivalent width (EW) of the emission nor the flux of the $H\alpha$ line alone are the parameters that controls the detection limit in prism surveys. Moss et al. (1988) introduced an auxiliary parameter defined as $EW \times Flux$, and showed that it defined accurately the observational limit of their work, an objective-prism survey in the red region of the spectrum, at a reciprocal dispersion of 400 \AA mm^{-1} . We have also used this parameter in our survey. In figure 5 we show the histogram of values $EW(\text{\AA}) \times Flux(\text{erg s}^{-1} \text{ cm}^{-2})$ for the sample of UCM galaxies from Lists 1 & 2. We can conclude that the UCM survey is able to identify emission-line galaxies with a value of $\log(EW \times Flux) > -13$. Only four objects have lower values of this parameter. Nevertheless three of them have redshifts larger than the limit imposed by the emulsion sensitivity, being impossible to register the $H\alpha$ emission. These objects must be considered as serendipitous identifications.

In figure 6 we show the distribution of the UCM objects of the Lists 1 & 2 in a $\log(Flux)$ vs. $\log(EW)$ plot. The data have been obtained from the work of Gallego et al. (1996). The plot shows the behavior of a sample obtained by prism plates. It also shows the lack of galaxies in the upper-left and lower-right corners. These two regions belong to very bright and faint galaxies respectively. Therefore the diagram shows that, in addition to a limiting magnitude, there exists a deficiency of bright galaxies due to saturation of the photographic plates. We can not represent the location of the galaxies obtained in this List 3 until performing spectroscopic observations. Nevertheless, these effects are due not to the visual or automatic procedure to select the candidates, but to the intrinsic characteristics of the photographic emulsion. This is why we expect a similar response for the galaxies identified in this list.

6. Statistical properties⁶

6.1. Apparent magnitudes

The histogram of apparent magnitudes presented in figure 7 informs us about the depth of the survey. Nearly all the galaxies lie between 16 and 18 in B magnitude, with a few reaching magnitude 20. The mean apparent B magnitude for the sample is 16.8. This histogram shows a known bias of this technique, that

⁶For now on, we adopt a value of $H_0=50 \text{ km s}^{-1} \text{ Mpc}^{-1}$ and $q_0=0.5$.

is, it is unable to detect bright galaxies because they appear saturated in the photographic plates. This occurs, for example, for several known galaxies as NGC 5637 ($m_B=14.7$) or WAS 82 ($m_B=15.5$). We also have presented the histogram of Gunn-Thuan r magnitudes obtained from the UCM Lists 1 & 2. Assuming a mean color $B-r=0.65$ for the UCM sample of galaxies, a typical value for Scd galaxies (Fukugita et al. 1995; Vitores et al. 1996b), the comparison points out that UCM List 3 seems to be slightly deeper than the previous ones, although lack of precision in our B magnitudes prevents us from extending these conclusions. We note that the large number of galaxies in the UCM List 1 & 2 histogram is due to the greater explored area compared with this List 3.

6.2. Absolute magnitudes

Figure 8 shows the histogram in absolute magnitude. The mean absolute magnitude is $M_B = -18.9$. This histogram is less symmetrical than the distribution of M_r derived from Lists 1 & 2 (Vitores et al. 1996b). Our coverage of the low luminosity end of the luminosity function is by far better than previous UCM lists. It is worth noting that galaxies with M_B as faint as -15 have been detected. Such percentage of low luminosity galaxies has been also reached for the University of Michigan survey for emission-line galaxies (MacAlpine et al. 1977).

6.3. Surface brightness

We have computed the mean surface brightness using the apparent blue magnitude and the size referred to the isophote $25 \text{ mag arcsec}^{-2}$. The mean surface brightness of our sample is distributed almost uniformly from 21.5 to $24.5 \text{ mag arcsec}^{-2}$ with 22.8 being the mean value (see figure 9). Lists 1 & 2 yield a mean surface brightness of $22 \text{ mag arcsec}^{-2}$ in the Gunn-Thuan r band (Vitores et al. 1996b). The precision of our data prevents us to extend this study to filter or color differences.

In figure 10 we plot B magnitude vs. surface brightness for the sample. The BCD type galaxies are mainly distinguished because of their low luminosity and high surface brightness. The right side of the plot is populated by such galaxies. Considering an upper limit of $M_B > -18$ (Thuan & Martin 1981) for a BCD galaxy, we have regarded those galaxies with a compact aspect and a more conservative $M_B > -16.5$ as good candidates to be

BCD galaxies. Attending to this criteria the most probable candidates for BCD's are: UCM1345+2417, UCM1413+2446, UCM1449+2559, UCM1735+2617, UCM1742+2343 and UCM1742+2634. Other type of galaxies found in this region are irregular galaxies with strange morphologies such as comet-like shapes, double-component, etc. Such galaxies are UCM1640+2238, UCM1721+2326, UCM1723+2556 and so they were not included in the BCD sample.

6.4. Spatial distribution

In figure 11 we show the spatial distribution of our sample for both the 14^h and the 16^h regions. The dots represent galaxies from the CfA survey (Huchra, Geller & Corwin 1995) which have been plotted to show for the normal galaxy distribution. It can be seen that several clustering structures appear in the CfA data. A well-defined cluster is at 5000 km/s and three more at 9000 km/s , 9500 km/s and 11000 km/s (beyond the UCM instrumental limit in redshift) in the 14^h field. In the 17^h sector only one cluster is observed at 10000 km/s . At such redshift, we detect no galaxies.

We have presented the location of the UCM galaxies using open circles. They nearly follow the distribution of the CfA survey, although less clustering seems to appear. Preliminary analysis points out the idea that preferred galaxy location could be related with physical size.

7. Comparison with other surveys

The UCM Survey has found 113 candidates in the 9 fields (189 deg^2) of this List 3. The overall density is around 0.59 candidates per square degree, slightly greater than the value derived from UCM Lists 1 & 2. It is worth noting that the actual density of galaxies with $H\alpha$ emission (excluding candidates with no emission) is ~ 0.4 for the first lists (Gallego et al. 1996). One of the properties of the automatic method is a better success rate of detection (Alonso 1996) (which will be determined for this survey with follow-up spectroscopy). Therefore this value is consistent with an improvement in the number of galaxies detected. Although we have lost some bright and extended galaxies, at fainter magnitudes the automatic procedure is more sensitive, providing an increase in the number of galaxies per square degree.

In Lists 1 & 2 some comparisons were made between the samples detected with different surveys and

observational techniques, and that obtained by us. The conclusions we derived do not change when the new UCM fields surveyed are added to the comparison. Following Kinman (1984) the CGCG galaxies have been used as the reference sample of galaxies in the field. Only 26 galaxies out of 242 galaxies with known redshift $z \leq 0.04$ have been found with emission. The ratio is $\sim 11\%$, similar to the 13% found in the previous lists.

The UCM List 3 fields do not overlap completely with the KUG survey (Kiso ultraviolet-excess galaxies, Takase et al. (1993)). If we restrict our analysis to the common region ($13^h45^m - 14^h30^m$), the KUG survey has found 94 objects and UCM 26 candidates; only 7 have been selected by both surveys. Thus only 27% of UCM galaxies are also KUG objects. Since the KUG survey selects objects by their colors, it is not redshift limited. We expect that a fraction of the KUGs have a redshift that prevents detection by us. For comparison Comte et al. (1994) found 25% of KUGs with $z > 0.04$. The number density of KUGs is 1.8 objects per square degree for the total survey and outnumber the surface density of UCM by a factor of 3.

There are 5 galaxies of the Wasilewski (1983) catalogue of emission-line galaxies that have been also detected by our survey. Although the detection technique is similar (objective-prism), he used IIIaJ emulsion to register $H\beta$ and [OIII] lines. The one galaxy undetected by us is WAS82 ($m_B=15.5$) due to a saturation problem (see §6).

8. Summary

We have presented the UCM survey List 3. This new research is the scientific continuation of the previous two lists, but in this last list we have applied an automatic procedure developed and tested by us in a previous work in order to improve the results obtained up to now with the visual search of candidates. This List 3 covers 189 sq. deg. in nine fields, and yields a total number of 113 candidate $H\alpha$ emission-line galaxies, giving an overall density of 0.59 candidates per square degree.

The nine fields were acquired in direct and objective-prism modes, and the plates were scanned using the MAMA machine. This procedure has permitted us to recover a great amount of information directly from the plates, allowing to perform statistical analysis of the sample before carrying out photometric or spec-

troscopic observations. We have derived high precision coordinates, magnitudes in the blue band, sizes and redshifts for the whole sample of candidates, all with moderate and known errors. Because we work with uncalibrated plates, all these parameters are obtained by comparing our photographic data with several parameters for objects recovered from various databases. These external calibrations allow for the determination of the parameters noted above.

The determination of the dispersion curve of the prism used in the survey has permitted us to estimate the redshift for the whole sample of candidates by measuring the position of the $H\alpha$ line in the prism spectrum related to the location of a constant reference point obtained using the astrometric calibration. The $1 - \sigma$ error in the computation of the redshift by this method results 0.004 (1200 km s^{-1}). The comparison with known objects shows the precision of the method developed.

The photometric data obtained for the sample (apparent and absolute magnitudes and sizes) follow the behavior derived for the two previous lists using specific photometric observations. This result suggests that the automatic procedure selects a sample of galaxies comparable with those obtained in the previous lists.

The success of the new automatic procedure adopted in this new third list is both the establishment of objective criteria for the selection of candidates and the extraction of several quantitative parameters, in comparison with the lack of such information from previous visual-based lists.

We would like to gratefully acknowledge the inestimable observation support received from the Calar Alto Observatory staff, specially from Kurt Birkle. We also express our thanks to Jean Guibert and the MAMA staff for their friendly assistance and warm hospitality. We would like to thank to Armando Gil de Paz, Javier Cenarro and Nicolás Cardiel for their helpful comments and valuable suggestions. We would also like to thank the anonymous referee for his useful suggestions and comments that improved this paper. This work has made use of the NASA/IPAC Extragalactic Database (NED), which is operated by the Jet Propulsion Laboratory, Caltech, under contract with the National Aeronautics and Space Administration. This research was supported in part by the Spanish Programa Sectorial de Promoción General del Conocimiento under grants

PB93–456, PB96–0065, PB96–0610.

REFERENCES

- Alonso O., Zamorano J., Rego M., Gallego J. 1995, A&AS, 113, 399
- Alonso O. 1996, PhD. Thesis, Universidad Complutense de Madrid.
- Alonso-Herrero A., Aragón-Salamanca A., Zamorano J., Rego M. 1996, MNRAS 278, 417
- Birkle, K. 1984 in “Astronomy with Schmidt-Type Telescopes”, M. Capaccioli ed., IAU coll.78, p.203
- Berger J., Cordoni J. P., Fringant A. M., Guibert J., Moreau O., Reboul H., Vanderriest C. 1991, A&AS 87, 389
- Comte G., Augarde R., Chalabaev A., Kunth D., Maehara H. 1994, A&A285, 1
- Fisher K. B., Huchra J. P., Strauss M. A., Davis M., Yahil A., Schlegel D. 1995, ApJS 100, 69
- Fukugita M., Shimasaku K., Ichikawa T. 1995, PASP 107, 945
- Gallego J., Zamorano J., Aragón-Salamanca A., Rego M. 1995, ApJL 455, L1
- Gallego J., Zamorano J., Rego M., Alonso O., Vitores A. G. 1996, A&AS120, 323
- Gallego J., Zamorano J., Rego M., Vitores A. G. 1997, ApJ 475, 502
- Gil de Paz A., Aragón-Salamanca A., Zamorano J., Gallego J., Alonso-Herrero A. 1998, (in preparation)
- Guibert J., Moreau O. 1991, The Messenger 64, 69
- Huchra J. P., Geller M. J., Corwin H. G. J., 1995, ApJS 99, 391
- Kinman T. D. 1984, in IAU Colloq. 78, Astronomy with Schmidt-Type Telescopes, ed M., Capaccioli (Dordrecht: Reidel), 409
- Kroll P., Neugebauer P. 1993, A&A 273, 341
- MacAlpine G. M., Smith S. B. & Lewis D. W. 1977, ApJS 34, 95
- Moreau O. 1992, PhD thesis, Université Paris 7
- Mohan V., Créze, 1987, A&A 68, 529
- Moss C., Whittle M., Irwin M. J. 1988, MNRAS 232, 381
- Paturel G., Fouqué P. Bottinelli L., Gouguenheim L. 1989, A&A 80, 299
- Paturel G., Fouqué P., Lauberts A., Valentijn E. A., Corwin H. G., de Vaucouleurs G. 1987, A&A 184, 86
- Reid N., Gilmore G. 1982, MNRAS 201, 73
- Roeser S., Bastian U. 1991, PPM Star Catalogue (Spektrum Akademischer Verlag, Heidelberg, Berlin, New York)
- Surace C., Comte G., 1994 A&A 281, 653
- Takase B., Miyauchi-Isobe N. 1993, Publ. Natl. Astron. Obs. Japan 3, 169.
- Thuan T. X., Martin G. E., 1981, ApJ 247, 823
- de Vaucouleurs G. 1984, in IAU Colloq. 78, Astronomy with Schmidt-Type Telescopes, ed M., Capaccioli (Dordrecht: Reidel), 409
- Vitores A. G., Zamorano J., Rego M., Alonso O., Gallego J. 1996a, A&AS 118, 7
- Vitores A. G., Zamorano J., Rego M., Gallego J., Alonso O. 1996b, A&AS 120, 385
- Wasilewski A. J. 1983, ApJ 272, 68
- Zamorano J., Rego M., Gallego J., Vitores A. G., González-Riestra R., Rodríguez-Caderot G. 1994, ApJS 95, 387 (List 1)
- Zamorano J., Gallego J., Rego M., Vitores A. G., Alonso O. 1996, ApJS 105, 343 (List 2)

Fig. 1.— Schematic map of the sky showing the field covered by the UCM List 3. Field centers are provided in table 1.

Fig. 2.— Relationship between the sizes for a small sample of galaxies taken from ECIS catalogue and those measured in our direct plates. Major and minor axis values are represented by squares and crosses respectively. The straight line represents the best fit. See §4.2 for details.

Fig. 3.— Dispersion curve for the 4° objective prism of the Schmidt Telescope at the Calar Alto Observatory. The bottom plot shows the position of some spectral features measured in A-type stars relative to the $H\beta$ line vs. wavelength. The curve displays the best fit assuming a refraction index law $n(\lambda)=a+b/\lambda^2$. The top diagram shows the dispersion dependence with wavelength.

Fig. 4.— Relationship between the redshift obtained from the prism spectra, applying the method described in §4.3, and those recovered from the literature for a small subsample of ELGs.

Fig. 5.— Histogram of values $EW \times Flux$ (of the $H\alpha$ emission line) for the sample of galaxies from UCM Lists 1 & 2.

Fig. 6.— $H\alpha$ Flux vs. EW for the sample of galaxies from UCM Lists 1 & 2. Solid line connect the points with the parameter $EW \times Flux$ constant. Dashed lines show the location of galaxies with continuum flux (in $\text{erg s}^{-1} \text{cm}^{-2} \text{\AA}^{-1}$) constant.

Fig. 7.— Histograms of apparent magnitudes from UCM Lists 1 & 2 (dashed line; Gunn-Thuan r magnitudes) and UCM List 3 (solid line; B magnitudes).

Fig. 8.— Histogram of absolute B magnitudes obtained for UCM List 3.

Fig. 9.— Histogram of mean B surface brightness inside the 25 mag/arcsec^2 isophote.

Fig. 10.— Surface brightness vs. absolute magnitude in the B band. Dashed lines represent galaxies with constant diameter size. Blue Compact Galaxy candidates are marked with a star.

Fig. 11.— Redshift-position diagrams for candidates of UCM List 3. The slices cover 6° centered at 24.5° in declination. Dots represent galaxies from the CfA survey while open circles show the UCM galaxies.

Fig. 12.— Finding charts for UCM galaxies of List 3. Each field covers a square $5'$ wide. Object is centered in the frame.

TABLE 1
PLATE DATA

Plate Ident. OP/Direct	Plate Center (J2000)		Common Field	Seeing (") OP/Direct	Number of Objects ELGs	
RA	DEC					
A516/A503	14 46 56	+23 59 27	$4.15^\circ \times 5.14^\circ$	1.0/1.5	14213	13
A513/A510	14 29 15	+23 53 45	$4.24^\circ \times 5.20^\circ$	2.5/1 .0	14932	14
A495/A507	14 13 12	+23 49 25	$3.92^\circ \times 5.04^\circ$	1.5/1 .0	16999	9
A497/A506	13 56 38	+23 57 39	$4.06^\circ \times 5.13^\circ$	2.0/1.0	17321	25
A496/A505	17 40 52	+24 23 34	$4.15^\circ \times 4.92^\circ$	1.5/2 .0	85601	19
A498/A509	17 23 17	+24 33 57	$4.15^\circ \times 5.05^\circ$	2.0/1.0	75618	13
A500/A504	17 05 55	+24 30 09	$4.07^\circ \times 5.15^\circ$	1.0/1.0	47559	10
A514/A508	16 50 01	+24 04 37	$4.13^\circ \times 5.17^\circ$	2.5/1 .0	27558	5
A517/A512	16 32 24	+24 04 30	$4.07^\circ \times 5.13^\circ$	1.0/1.0	29583	5

TABLE 2
UCM SURVEY LIST 3

UCM (1)	RA (2)	DEC (3)	m_B (4)	Size (5)	PA (6)	Redshift (7)	Morph (8)	OP emission (9)	Other names (10)
1345+2417	13 48 06.3	24 02 21	17.0	18×14	143	0.004	C	w	
1345+2457	13 47 36.5	24 42 13	17.0	18×17	0	0.024	I	m	
1346+2420	13 49 18.2	24 05 45	16.0	37×18	111	0.021	I	m	
1347+2527	13 49 37.6	25 13 04	18.0	8×7	72	0.023	*	m	
1348+2147	13 51 17.8	21 32 38	15.2*	35×30	99	0.025	S_f	w	KUG 1348+217
1348+2510	13 50 20.2	24 56 09	17.0	24×12	2	0.031	S	s	IRAS F13480+2511
1349+2151	13 51 24.8	21 36 19	17.0	14×11	58	0.038	*	s	
1349+2152	13 51 38.0	21 37 39	16.5	36×13	161	0.031	S_e	m	IRAS F13492+2152
1350+2207	13 53 20.3	21 53 09	16.5	21×13	172	0.033	I	m	
1350+2456	13 52 26.5	24 41 29	19.0	6×4	105	0.029	*	m	
1350+2529	13 52 24.9	25 14 47	17.0	17×12	53	0.032	O	m	
1351+2201	13 53 25.7	21 46 17	17.0	14×11	108	0.036	O	s	
1351+2521	13 53 38.7	25 06 41	17.0	20×11	109	0.027	S_e	w	
1352+2202	13 54 58.8	21 48 17	16.0	24×19	29	0.036	S_f	m	
1352+2256	13 54 39.2	22 41 40	17.0	22×15	51	0.023	S_f	m	
1353+2507	13 55 37.3	24 52 37	17.0	16×12	82	0.030	O	w	
1353+2517	13 55 34.4	25 02 59	16.09*	35×21	21	0.0295*	S_f	w	CGCG 132-048
1353+2531	13 55 36.1	25 16 27	17.0	17×9	97	0.023	S_e	m	
1353+2647	13 55 38.0	26 32 51	17.02*	16×10	112	0.009	S_f	w	NPM1G +26.0340
1355+2440	13 57 37.8	24 26 04	17.0	15×10	69	0.032	C	m	
1356+2157	13 58 36.2	21 43 16	16.0	46×16	18	0.032	S_e	s	
1356+2310	13 58 24.7	22 55 39	15.5	29×21	127	0.017	S_f	m	
1357+2614	14 00 12.0	26 00 21	18.5	12×8	108	0.020	I	m	
1400+2304	14 03 05.9	22 50 26	17.41*	28×13	57	0.019	S	w	NPM1G +23.0349
1401+2602	14 04 01.8	25 47 44	14.9*	18×15	115	0.0330*	O	s	WAS 89
1402+2152	14 04 53.0	21 38 09	14.9*	38×29	95	0.0165*	S	w	MRK 0667
1408+2543	14 10 57.2	25 29 48	14.43*	71×64	92	0.0316*	S_f	w	IC 4381
1408+2547	14 10 54.2	25 33 14	15.9*	20×16	84	0.0312*	S_f	m	WAS 90
1408+2623	14 10 28.5	26 09 05	16.0	18×17	48	0.029	C	m	
1413+2317	14 15 22.3	23 03 50	17.0	22×13	106	0.023	S	m	
1413+2446	14 15 27.3	24 32 26	20.0	7×5	118	0.024	*	m	
1416+2202	14 18 42.9	21 49 09	15.0	78×38	164	0.031	I_{IP}	s	UGC 09164
1416+2300	14 19 07.5	22 46 19	17.15*	19×18	175	0.019	S	m	NPM1G +23.0356

TABLE 2—*Continued*

UCM (1)	RA (2)	DEC (3)	m _B (4)	Size (5)	PA (6)	Redshift (7)	Morph (8)	OP emission (9)	Other names (10)
1416+2543	14 18 25.4	25 30 04	15.7*	62×18	28	0.0150*	S _e	w	KUG 1416+257
1418+2209	14 20 46.6	21 56 14	14.3*	16×32	154	0.0156*	S _e	m	UGC 09182
1419+2420	14 21 52.9	24 06 27	15.6*	30×20	72	0.020	S	m	KUG 1419+243
1422+2321	14 25 00.0	23 07 32	16.0	23×22	106	0.017	S _f	s	KUG 1422+233
1422+2450	14 24 22.9	24 36 52	14.11*	93×45	134	0.0171*	S _B	m	NGC 5610
1424+2515	14 26 26.8	25 01 47	17.0	14×12	94	0.022	O	w	
1424+2537	14 26 19.8	25 24 03	15.5*	31×23	82	0.019	O	w	KUG 1424+256
1424+2541	14 26 15.5	25 27 59	16.5	14×13	94	0.017	*	w	
1425+2146	14 27 34.1	21 33 25	17.0	21×11	24	0.030	S	w	
1426+2322	14 29 10.9	23 08 55	18.0	10×10	108	0.023	C	w	
1427+2314	14 30 11.0	23 01 36	15.3*	39×32	120	0.0173*	S	w	MRK 0683
1429+2145	14 31 20.9	21 32 10	16.5	25×13	118	0.018	S	w	
1431+2441	14 33 20.3	24 28 04	17.0	27×12	33	0.034	S	w	
1432+2550	14 35 06.5	25 37 48	16.5	16×12	93	0.015	S	w	
1435+2249	14 38 10.4	22 36 27	16.5	14×14	17	0.025	S	w	
1436+2245	14 38 21.1	22 32 12	16.5	27×18	11	0.017	I	w	IRAS 14360+2245
1437+2148	14 39 58.5	21 35 59	16.5	36×15	35	0.031	S	m	LSBC F580-06
1438+2209	14 41 15.8	21 56 44	16.5	20×19	169	0.025	S _f	m	NPM1G +22.0467
1438+2239	14 40 54.9	22 27 08	17.0	22×12	144	0.014	S	w	IRAS F14386+2239
1438+2307	14 41 15.2	22 54 32	17.5	13×12	164	0.0339*	S	m	IRAS 14389+2307
1440+2521	14 43 02.7	25 09 08	16.16*	28×14	47	0.0319*	S	s	UGC 09489
1442+2248	14 44 35.5	22 35 38	17.5	14×13	120	0.025	S	m	
1446+2312	14 48 45.2	22 59 34	15.5	45×22	111	0.008	S _{IP}	w	IRAS F14465+2311
1447+2535	14 49 35.8	25 22 52	14.34*	46×45	99	0.0339*	S _f	m	UGC 09544
1448+2248	14 50 38.5	22 36 31	17.5	12×12	27	0.034	C	w	
1448+2256	14 50 37.8	22 44 06	15.7*	25×22	168	0.0215*	S	s	MRK 1388
1449+2559	14 51 33.2	25 46 58	19.0	7×6	4	0.021	C	m	
1450+2342	14 52 24.1	23 30 41	17.5	14×11	51	0.034	S	m	
1624+2359	16 26 23.7	23 52 41	17.0	20×14	22	0.040	S	m	IRAS 16242+2359
1627+2433	16 29 52.8	24 26 39	15.5*	35×34	142	0.0375*	I	m	VV 807
1628+2453	16 30 55.8	24 46 49	17.0	20×16	98	0.026	S	w	
1636+2632	16 38 02.6	26 27 04	15.93*	25×22	29	0.009	S	m	NPM1G +26.0432
1637+2417	16 39 26.1	24 11 59	17.48*	18×15	140	0.015	C	w	NPM1G +24.0414
1640+2238	16 42 38.5	22 33 10	17.5	32×11	37	0.011	I	m	
1640+2510	16 42 23.8	25 05 07	14.8*	89×28	161	0.0227*	S	m	UGC 10514
1643+2213	16 45 15.0	22 08 22	15.7*	41×23	12	0.0316*	S	w	CGCG 138-069
1647+2259	16 49 23.9	22 54 16	17.0	15×11	179	0.025	*	m	
1650+2551	16 52 31.8	25 46 25	15.94*	28×22	139	0.0348*	S	s	IRAS 16504+2551
1655+2532	16 57 23.4	25 27 57	16.61*	20×16	109	0.040	S	m	NPM1G +25.0438
1656+2413	16 58 33.1	24 08 51	18.0	17×11	166	0.019	I	m	
1656+2450	16 58 47.0	24 46 24	17.5	38×12	42	0.025	S	w	
1701+2535	17 03 05.1	25 31 48	17.0	16×13	163	0.039	*	s	
1701+2642	17 03 48.2	26 38 37	17.0	12×11	152	0.027	*	s	
1702+2314	17 04 59.9	23 10 10	16.0	34×25	72	0.0304*	S _f	w	CGCG 139-033
1706+2300	17 08 52.3	22 57 10	17.0	18×10	46	0.022	*	s	
1710+2316	17 12 45.9	23 13 28	14.15*	53×38	33	0.034	S _B	s	NGC 6315
1711+2427	17 13 12.3	24 23 42	19.0	14×6	110	0.035	I	w	
1712+2305	17 14 25.5	23 01 39	17.0	20×12	153	0.030	S	w	
1712+2306	17 14 30.0	23 03 38	15.1*	34×27	48	0.0295*	S	w	ARK 520
1714+2442	17 16 54.3	24 38 54	18.0	14×13	32	0.021	I	m	
1714+2541	17 16 42.6	25 38 03	15.7*	39×22	116	0.023	S	w	CGCG 140-004
1717+2428	17 19 34.6	24 25 31	18.0	12×12	15	0.028	O	s	
1717+2458	17 19 56.6	24 55 57	17.0	29×18	126	0.019	S _B	s	
1721+2326	17 23 29.0	23 23 36	17.5	25×22	23	0.005	I _{IP}	s	
1722+2500	17 24 45.4	24 58 17	14.2*	68×37	43	0.0276*	S	w	UGC 10837
1722+2656	17 24 50.7	26 53 32	17.0	29×26	144	0.031	S _f	w	
1723+2556	17 25 48.6	25 53 33	18.0	17×11	135	0.014	C _{IP}	w	
1725+2653	17 27 47.0	26 51 16	15.74*	31×26	161	0.0296*	S	w	VV 389
1726+2339	17 28 18.8	23 37 27	15.5	30×23	62	0.030	S	s	CGCG 140-031
1727+2549	17 29 33.6	25 46 48	18.0	12×12	121	0.021	I	m	
1729+2548	17 31 14.8	25 46 20	18.5	13×12	25	0.020	I	w	
1732+2414	17 34 49.5	24 12 29	18.5	10×8	136	0.019	C	w	
1732+2509	17 34 49.7	25 07 44	17.5	21×12	121	0.022	IP	m	

TABLE 2—*Continued*

UCM (1)	RA (2)	DEC (3)	m_B (4)	Size (5)	PA (6)	Redshift (7)	Morph (8)	OP emission (9)	Other names (10)
1733+2441	17 35 38.6	24 39 39	18.0	16×8	87	0.018	C	w	
1733+2554	17 35 14.3	25 52 31	17.5	11×9	11	0.028	C	s	
1734+2219	17 36 29.6	22 17 15	16.89*	21×16	31	0.015	S	m	NPM1G +22.0588
1734+2322	17 36 36.3	23 21 08	17.61*	20×14	94	0.025	S	w	NPM1G +23.0458
1735+2617	17 37 08.0	26 16 01	19.0	8×6	73	0.014	C	m	
1735+2622	17 37 48.0	26 21 18	16.51*	21×17	46	0.022	S	w	NPM1G +26.0460
1736+2458	17 38 27.2	24 57 13	15.1*	54×22	155	0.0209*	S	w	UGC 10926
1738+2544	17 40 14.4	25 43 05	18.0	11×10	134	0.018	I	m	
1739+2637	17 41 41.2	26 36 18	17.5	14×12	35	0.030	S	m	
1739+2639	17 41 46.8	26 38 00	17.5	26×10	149	0.023	S	m	
1740+2210	17 42 40.7	22 09 13	16.5	18×13	124	0.043	S	w	
1740+2351	17 42 45.1	23 50 30	17.5	22×11	138	0.028	S	w	
1742+2343	17 45 00.2	23 42 22	19.0	10×9	133	0.014	C	s	
1742+2634	17 44 40.1	26 33 25	19.5	10×8	94	0.025	C	w	
1744+2629	17 46 26.4	26 28 53	19.0	9×8	169	0.024	C	m	
1745+2235	17 47 18.5	22 34 41	17.0	17×12	48	0.025	S	w	
1746+2412	17 48 47.1	24 11 18	17.0	28×15	40	0.028	I	s	

^{(2),(3)}J2000.0 Equatorial Coordinates.

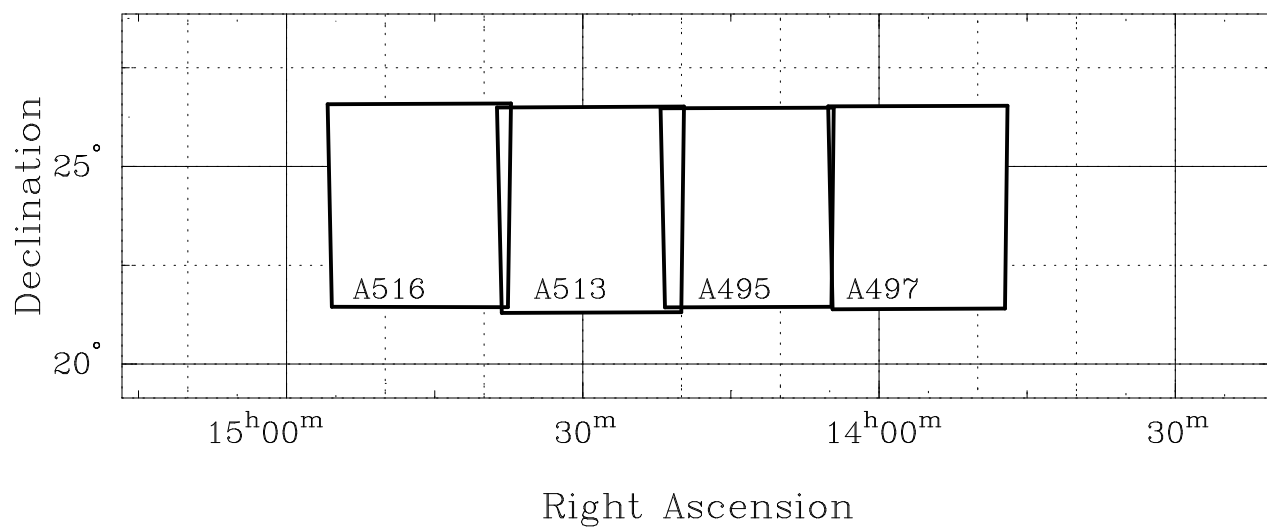
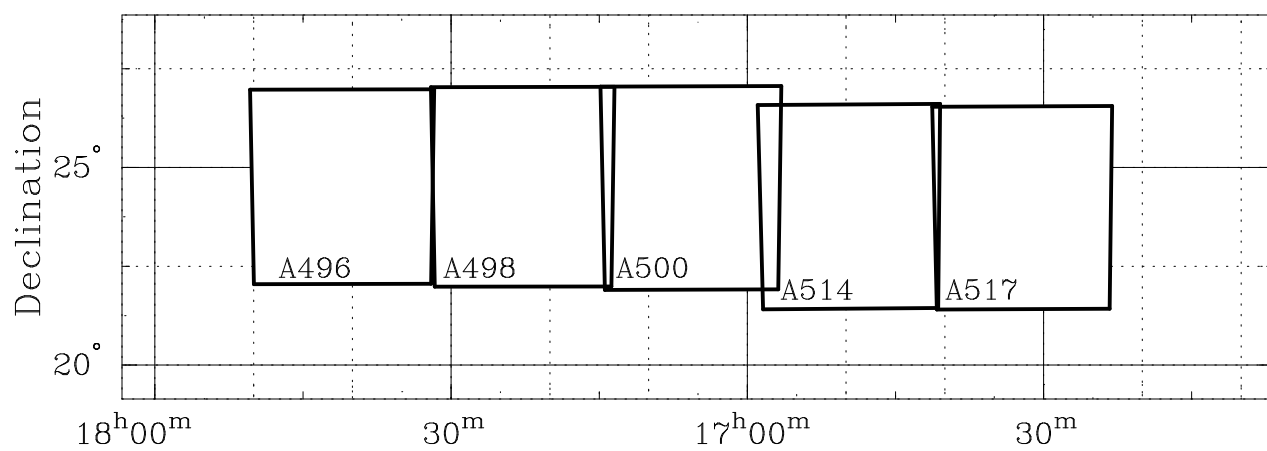
⁽⁴⁾Data obtained from literature are marked with an asterisk

⁽⁵⁾Sizes expressed in arcsec

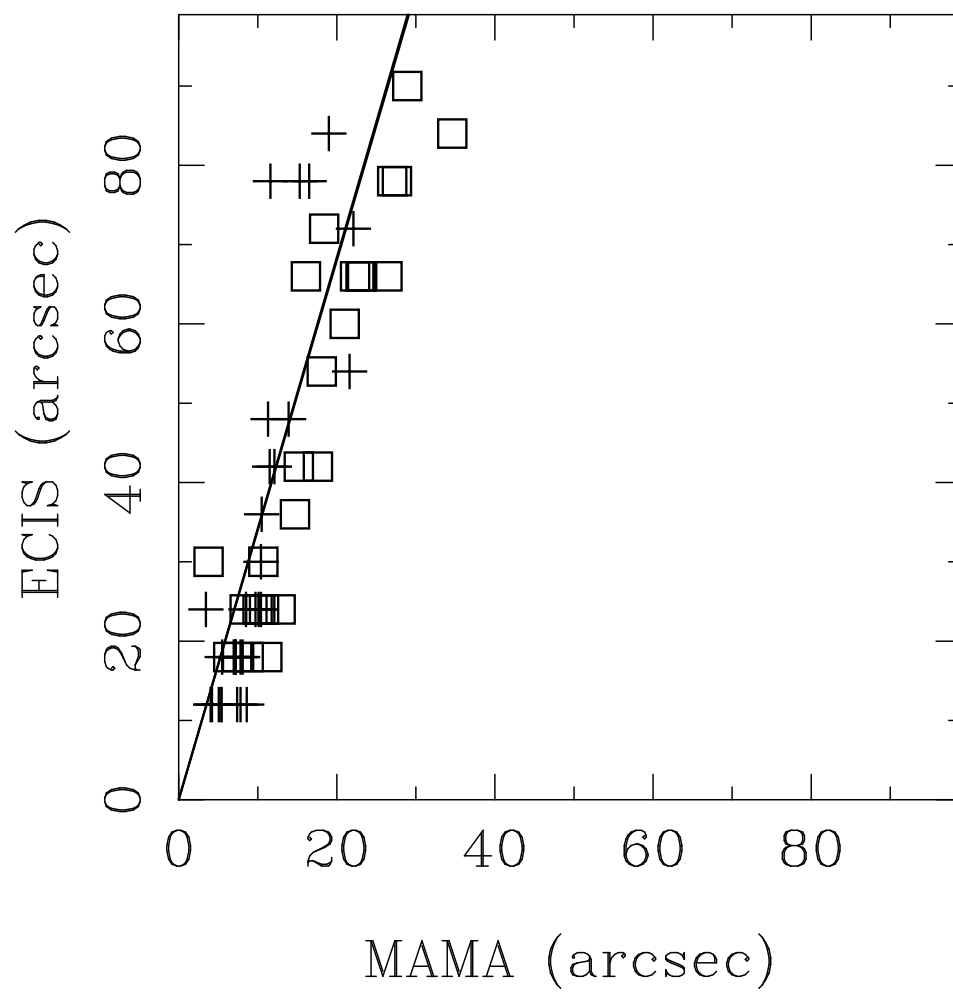
⁽⁷⁾Data obtained from literature are marked with an asterisk

⁽⁸⁾C: Compact; I: Irregular; O: Oval; IP: Interacting Pair; *: Stellar-like; S: Spiral [S_f : near face-on; S_e near edge-on; S_B : Barred spiral]

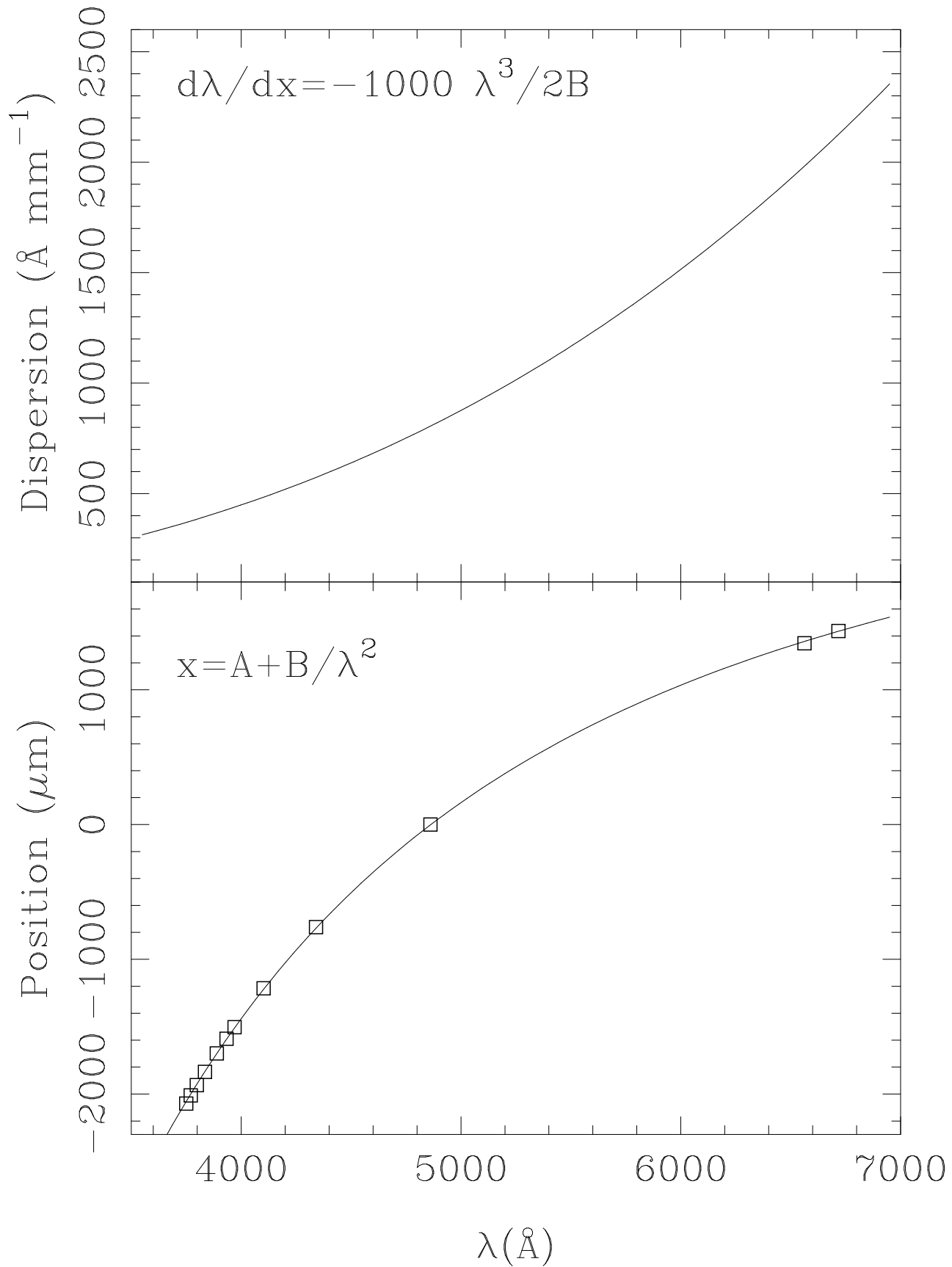
⁽⁹⁾Visual estimation of the H α emission (w: weak; m: medium; s: strong)



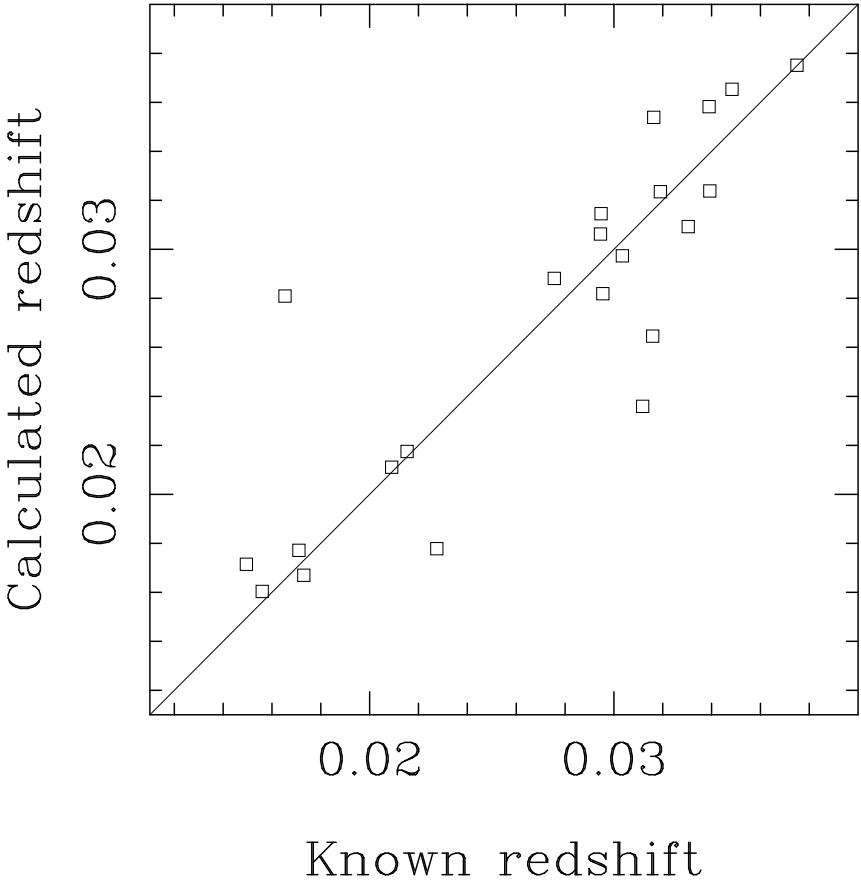
Size calibration

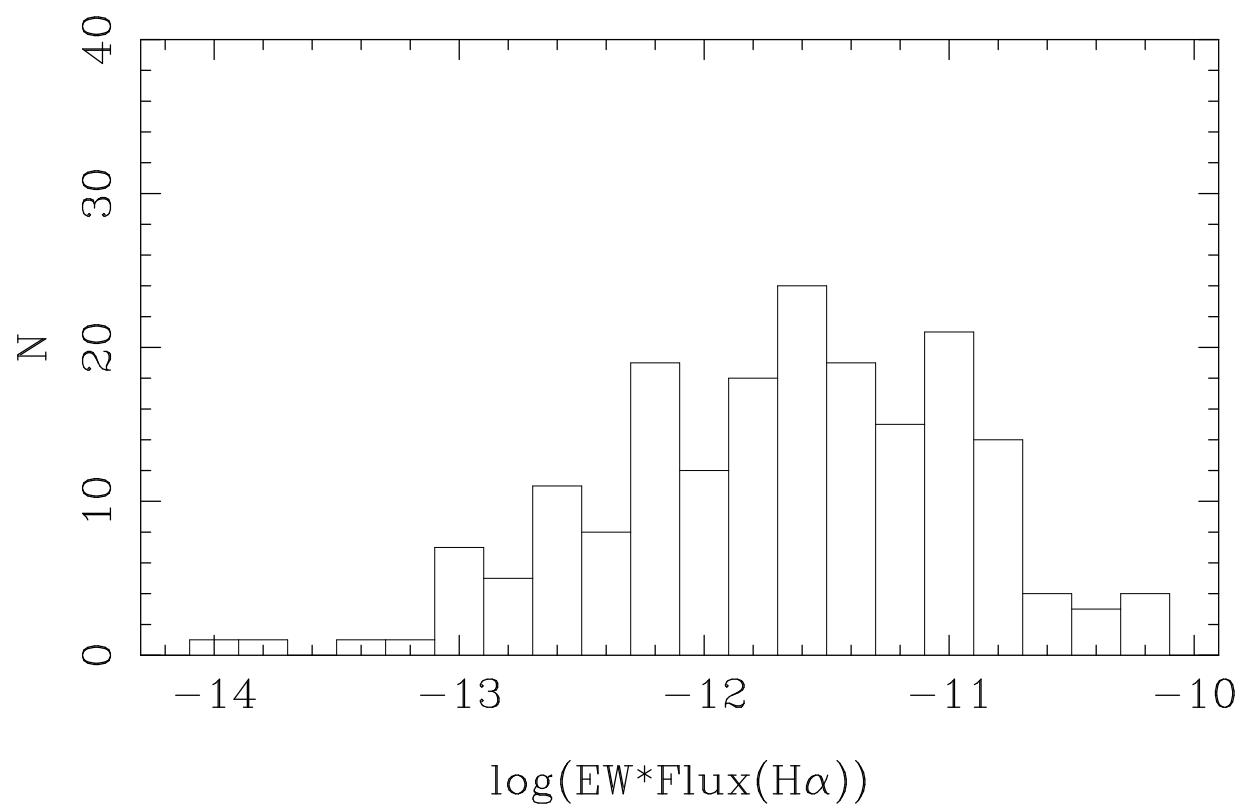


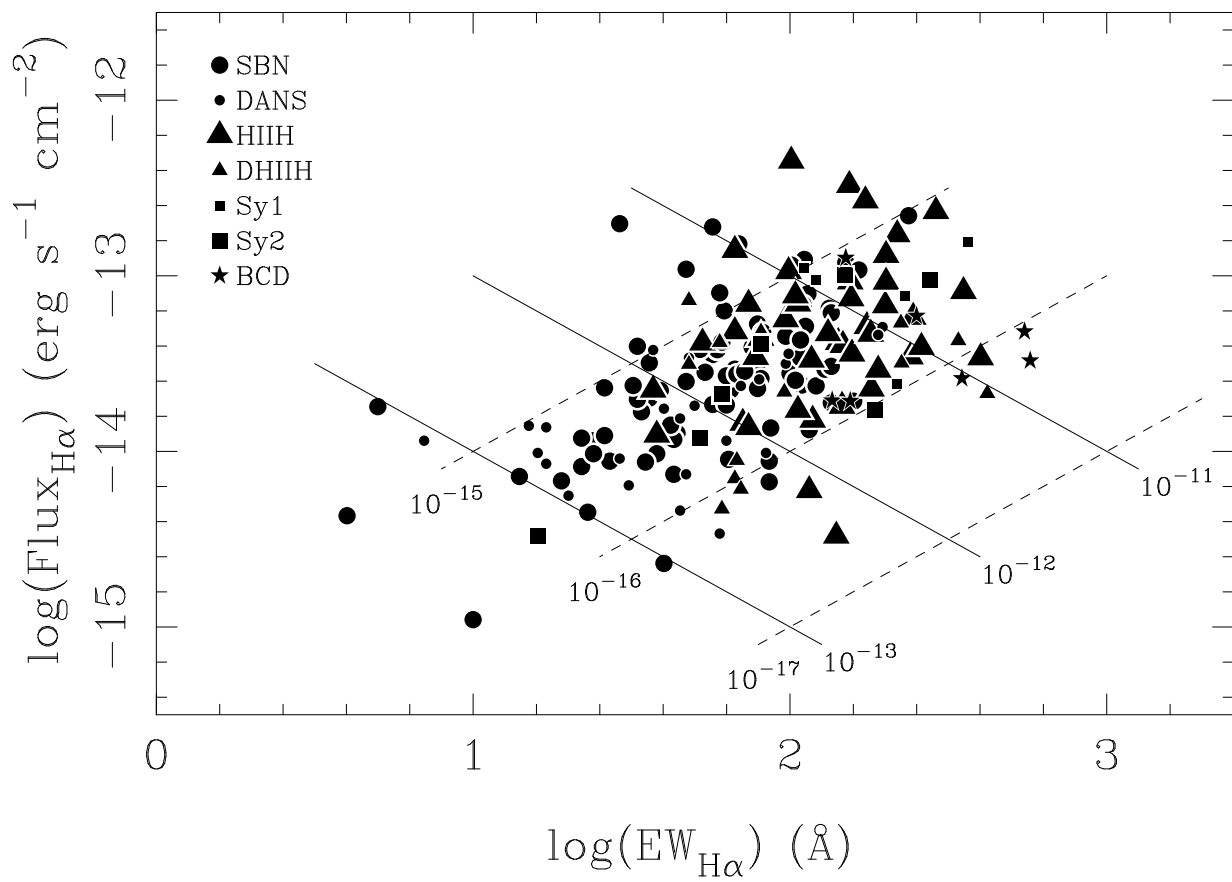
CAHA Schmidt Telescope. 4° Prism

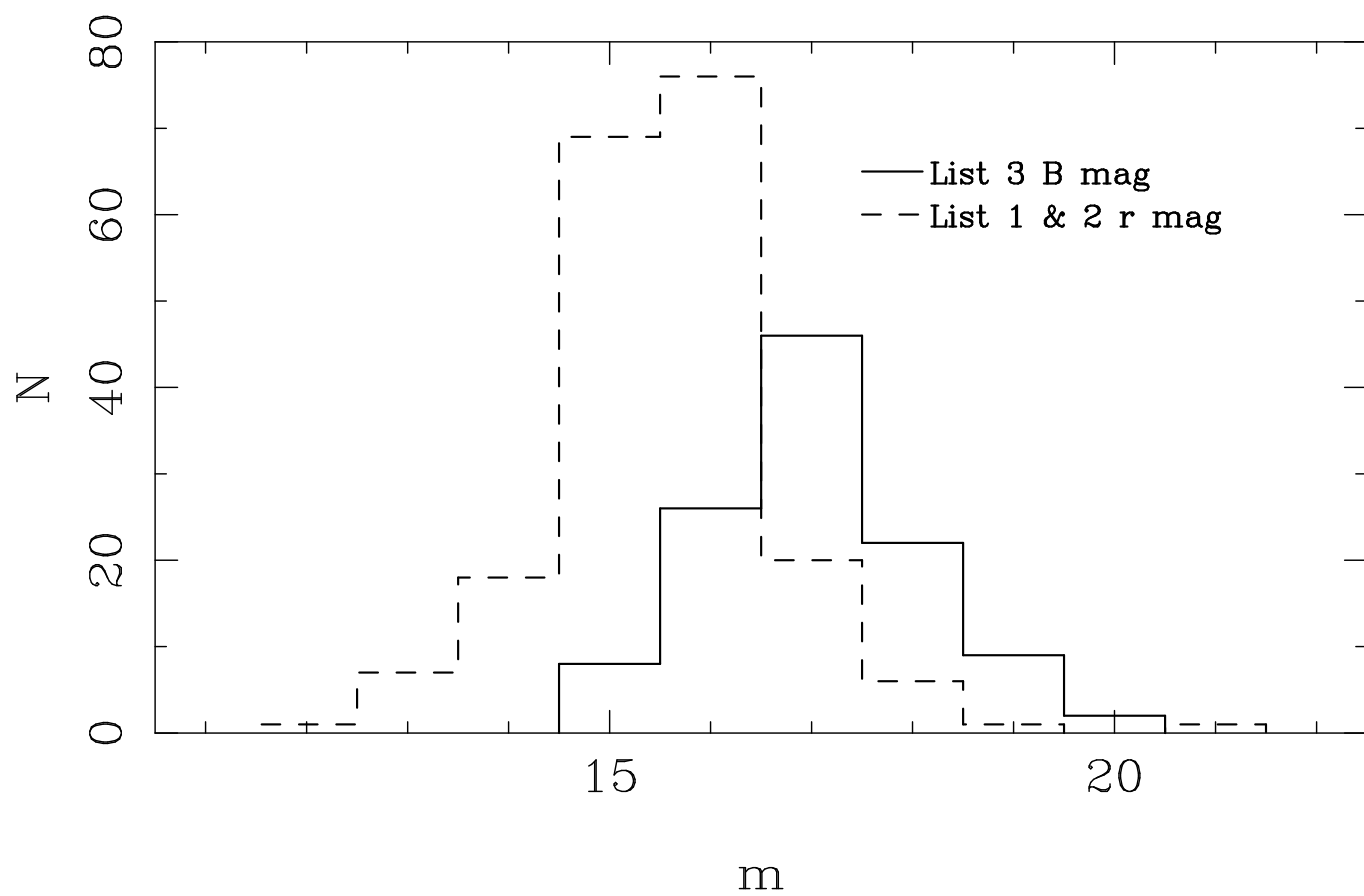


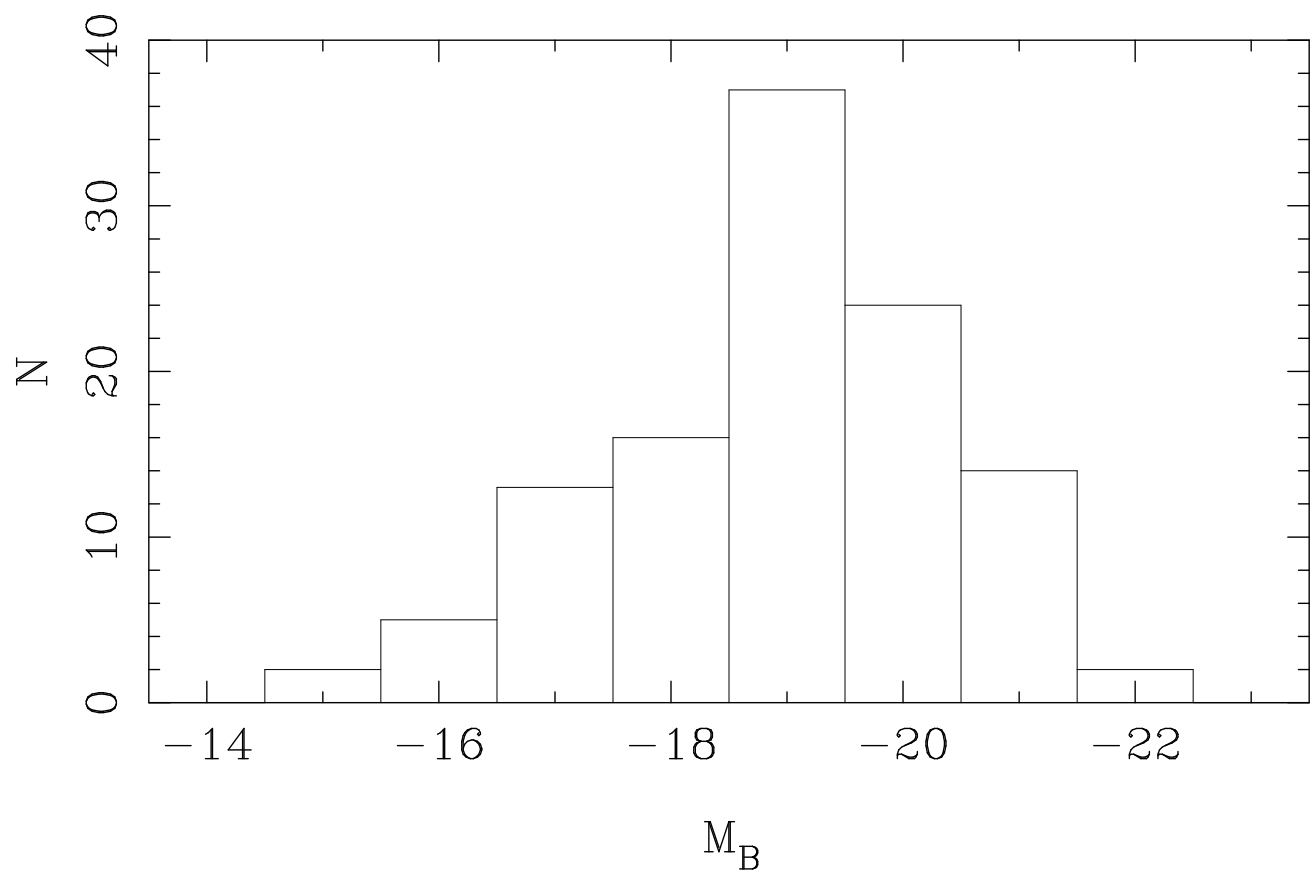
Redshift calibration

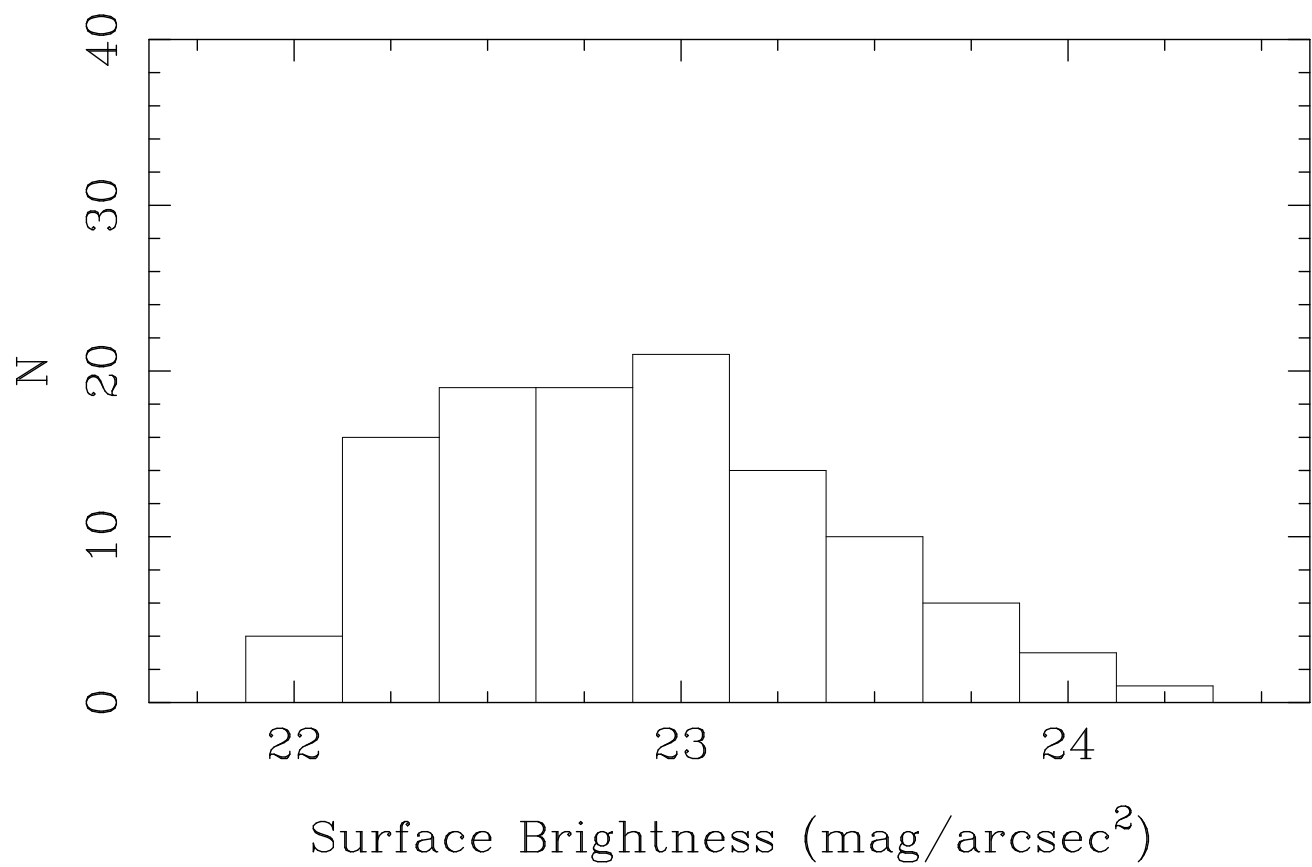




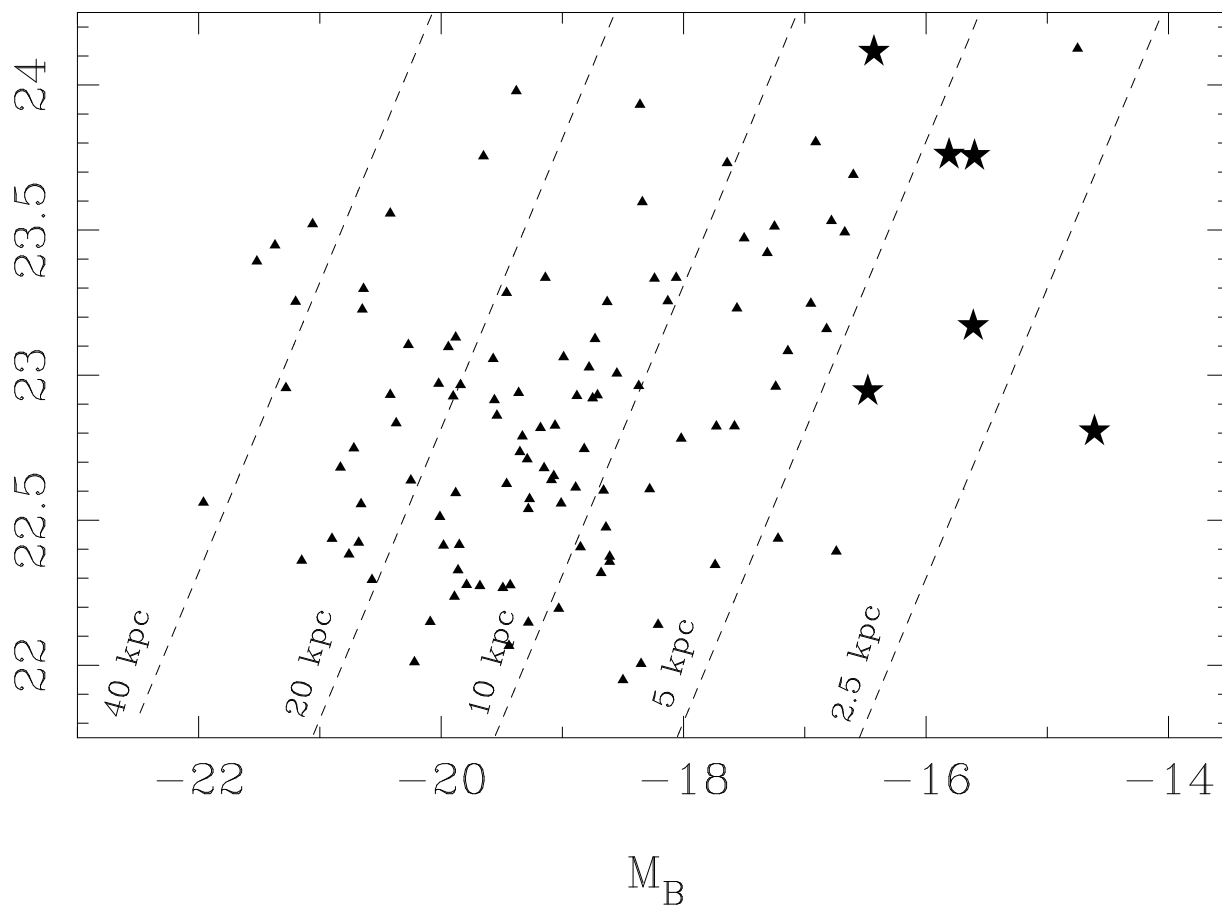






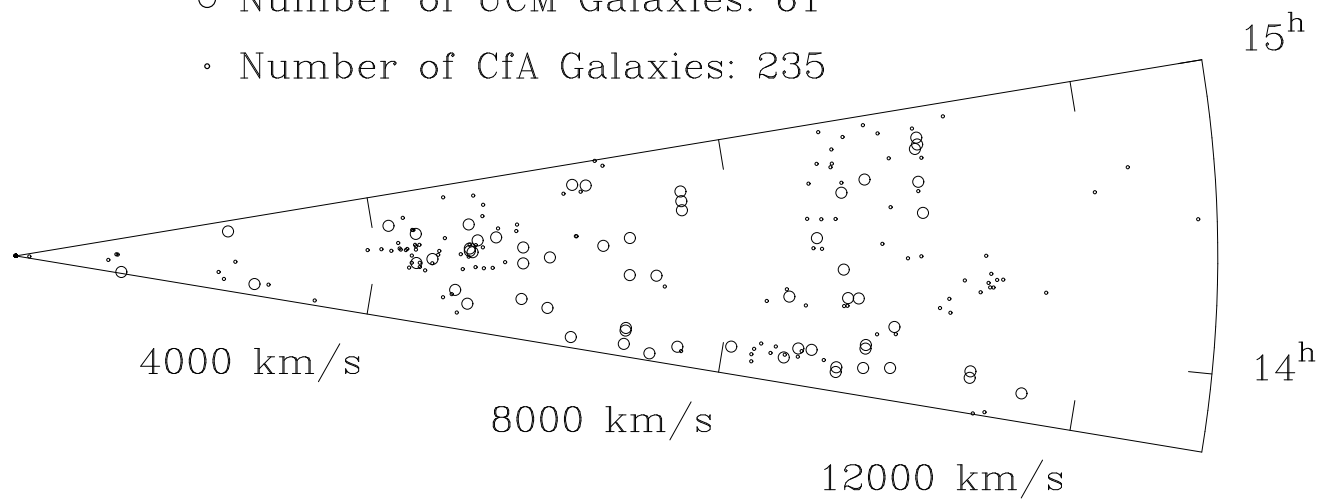


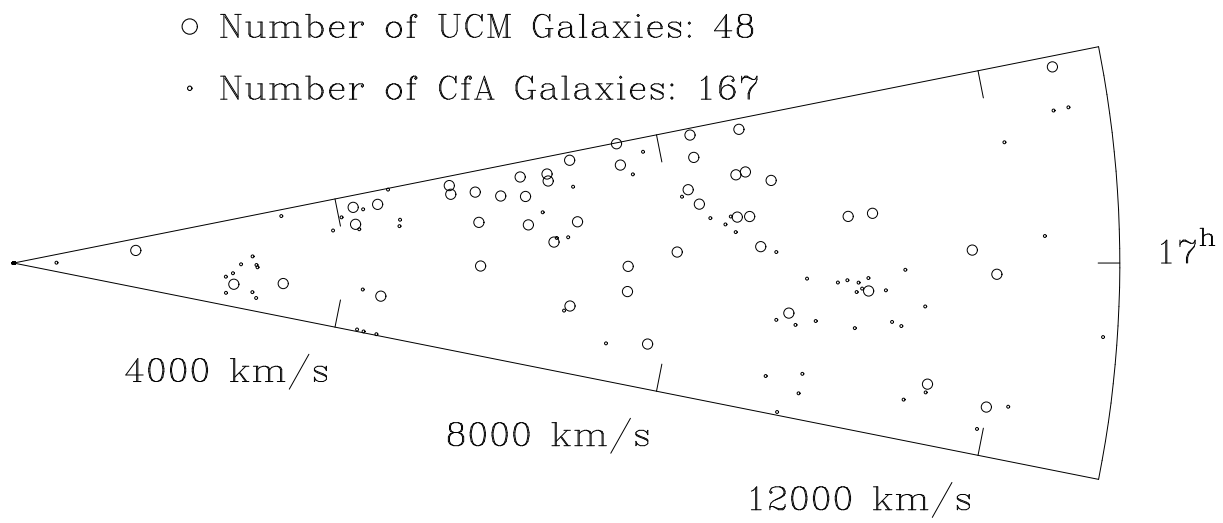
Surface Brightness ($\text{mag}/\text{arcsec}^2$)



○ Number of UCM Galaxies: 61

• Number of CfA Galaxies: 235





This figure "fig12a.jpg" is available in "jpg" format from:

<http://arxiv.org/ps/astro-ph/9901202v2>

This figure "fig12b.jpg" is available in "jpg" format from:

<http://arxiv.org/ps/astro-ph/9901202v2>

This figure "fig12c.jpg" is available in "jpg" format from:

<http://arxiv.org/ps/astro-ph/9901202v2>

This figure "fig12d.jpg" is available in "jpg" format from:

<http://arxiv.org/ps/astro-ph/9901202v2>

This figure "fig12e.jpg" is available in "jpg" format from:

<http://arxiv.org/ps/astro-ph/9901202v2>

This figure "fig12f.jpg" is available in "jpg" format from:

<http://arxiv.org/ps/astro-ph/9901202v2>